

Critical currents and vortex dynamics in percolative superconductors containing fractal clusters of a normal phase

Yuriy I. Kuzmin*

*Ioffe Physical Technical Institute of the Russian Academy of Sciences,
26 Polytechnicheskaya Street, Saint Petersburg 194021 Russia*

(Dated: September 27, 2018)

The effect of fractal clusters on magnetic and transport properties of percolative superconductors is considered. The superconductor contains percolative superconducting cluster, carrying a transport current, and clusters of a normal phase, which act as pinning centers. A prototype of such a structure is a high-temperature superconducting (HTS) wire. The superconducting core of first generation HTS wires is the conglomeration of superconducting micro-crystallites containing normal-phase clusters inside. There are the clusters of columnar defects in superconducting layer, which is the current-carrying element of second generation HTS wire. It is found that normal-phase clusters can have essential fractal features that affect the vortex dynamics. The fractal dimension of the boundary of normal-phase clusters in YBCO films is estimated and the cluster statistics is analyzed. Depinning and transport of vortices in fractal superconducting structures are investigated. Transition of the superconductor into a resistive state corresponds to the percolation transition from a pinned vortex state to a resistive state when the vortices are free to move. It is revealed that a mixed state of the vortex glass type is realized in the superconducting system involved. The fractal distribution of critical currents is derived and its peculiarities are studied. It is found that there is the range of fractal dimension where this distribution has anomalous statistical properties, specifically, its dispersion becomes infinite. The current-voltage characteristics of superconductors containing fractal clusters are obtained. Dependencies of the free vortex density on the fractal dimension as well as the resistance on the transport current are studied. It is found that the fractality of the cluster boundary intensifies pinning and thereby raises the critical current. This feature enables the current-carrying capability of a superconductor to be enhanced without changing of its chemical composition.

PACS numbers: 74.81.-g; 74.25.Fy; 74.81.Bd

I. INTRODUCTION

An essential feature of the clusters of defects in superconductor lies in their capability to trap a magnetic flux.^{1,2,3} Holding in place the vortices driven by the Lorentz force, such clusters can act as effective pinning centers.^{4,5} This feature can be used in making new composite superconducting materials of enhanced current-carrying capability.^{6,7,8} The cluster structure affects the vortex dynamics in superconductors, especially when clusters have fractal boundary.^{9,10,11,12,13} In the present paper the magnetic and transport properties of composite superconductors with fractal clusters of a normal phase will be considered as well as the phenomena limiting the current-carrying capability of such superconductors will be discussed.

A prototype of superconductor containing inclusion of a normal phase is a superconducting wire. The first generation high-temperature superconducting (HTS) wires are fabricated following the powder-in-tube technique (PIT). The metal tube is being filled with HTS powder, then the thermal and deformation treatment is being carried out. The resulting product is the wire consisting of one or more superconducting cores sheathed by a normal metal (Fig. 1). The sheath endows the wire with the necessary mechanical (flexibility, folding strength) and electrical (the possibility to release an excessive power when the superconductivity will be suddenly lost) prop-

erties. At present, the best results are obtained for the silver-sheathed bismuth-based composites, which are of practical interest for energy transport and storage. In view of the PIT peculiarity the first generation HTS wire has a highly inhomogeneous structure.¹⁴ Superconducting core represents a dense conglomeration of BSCCO micro-crystallites containing normal-phase inclusions inside (see inset in Fig. 1). These inclusions primarily consist of a normal metal (silver) as well as the fragments of different chemical composition, grain boundaries, micro-cracks, and the domains of the reduced superconducting order parameter.^{15,16,17} The volume content of a normal phase in the core is far below the percolation threshold, so there is a percolative superconducting cluster that carries the transport current.

The second generation HTS wires (coated conductors) have multi-layered film structure consisting of the metal substrate (nickel-tungsten alloy), the buffer oxide sub-layer, HTS-layer (YBCO), and the protective cladding made from a noble metal (silver). Superconducting layer, which carries the transport current, has the texture preset by the structure of an oxide sub-layer. In the superconducting layer there are clusters of columnar defects (see Fig. 2) that can be created during the film growth process as well as by the heavy ion bombardment.^{5,18} Such defects are similar in topology to the vortices, therefore they suppress the flux creep so it is possible to get the critical current up to the depairing value.^{1,19}

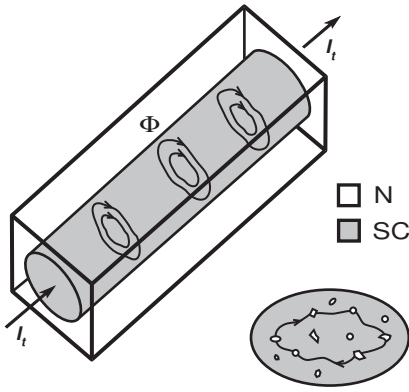


FIG. 1: Schematic representation for the first generation superconducting wire. The superconducting core is sheathed by the normal metal. The transport current creates the magnetic flux concentrated along irregular-shaped rings passing through the normal-phase inclusions. The inset shows the cross-section of the wire with normal-phase inclusions as well as one cluster defined as a set of pinning centers, which are united by the common trapped flux.

II. MAGNETIC FLUX TRAPPING IN PERCOLATIVE SUPERCONDUCTORS

Let us consider a superconductor containing inclusions of a normal phase, which are out of contact with one another. These inclusions may be formed by the fragments of different chemical composition, as well as by the domains of reduced superconducting order parameter. The columnar defects of such a kind can readily be created in superconducting film at the sites of defects on the boundary with the substrate (see Fig. 2). A passage of electric current through a superconductor is linked with the vortex dynamics because the vortices are subjected to the Lorentz force created by the current. In its turn, the motion of the magnetic flux transferred by vortices induces an electric field that leads to the energy losses. In HTS's the vortex motion is of special importance because of large thermal fluctuations and small pinning energies.²⁰ Here we will consider the simplified model of one-dimensional line pinning when a vortex filament is trapped by the set of pinning centers.²¹ A superconductor containing isolated clusters of a normal phase allows for effective pinning, because the vortices cannot leave them without crossing the surrounding superconducting space. The clusters present the sets of normal-phase inclusions, which are united by the common trapped flux and surrounded by the superconducting phase. The flux can be created both by an external source (e.g., during magnetization in field-cooling regime) and by the transport current (in self-field regime). The magnetic flux remains to be trapped in the normal-phase clusters till the Lorentz force created by the transport current exceeds the pinning force.

If the relative portion of superconducting phase exceeds the percolation threshold, there is a superconduct-

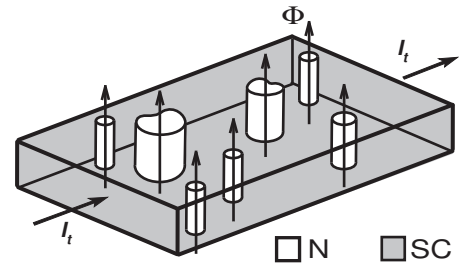


FIG. 2: Superconducting film with columnar clusters of a normal phase. Such a film represents the current-carrying element of the second generation superconducting wire (coated conductors).

ing percolation cluster carrying a transport current. In such a structure magnetic flux is locked in finite clusters of a normal phase (see Fig. 3(a)). If the transport current is passed through the sample, the trapped flux remains unchanged as long as the vortices are still held in the normal-phase clusters. The larger clusters have to allow for a weaker pinning than smaller ones, because the larger the cluster size, the more entry points into weak links, through which the vortices can pass, are located along its boundary. When the current is increased, the magnetic flux will break away first from the clusters of smaller pinning force, and therefore, of larger size. Magnetic flux trapped into a single cluster is proportional to its area A . Therefore, the decrease in the total trapped flux $\Delta\Phi$ is proportional to the number of the clusters of area larger than a preset value A . So that value can be expressed with the cumulative probability function $W(A) = \Pr\{\forall A_j < A\}$, which is equal to the probability to find the cluster of area A_j smaller than an upper bound of A :

$$\frac{\Delta\Phi}{\Phi} = 1 - W(A) \quad (1)$$

The left hand side of this formula is equal to the relative decrease in the total trapped flux caused by the transport current of the same amplitude as the depinning current of the cluster of area A , and the right hand side gives the provability to find the cluster of area greater than A in the whole population.

When the current is increased, the magnetic flux starts to break away from the clusters of pinning force weaker than the Lorentz force created by the transport current. The vortices, driven by this force, must cross the surrounding superconducting space, and they will first do that through the weak links, connecting the normal-phase clusters (see Fig. 3(a) where weak links are shown by the black curves connecting the white normal-phase clusters). In such a system depinning has a percolative character,^{22,23,24} because unpinned vortices move through the randomly generated channels created by weak links. In Fig. 3(b) the equivalent weak-link-network circuit representation of such a system is shown. The normal-phase clusters are presented by the cells of the

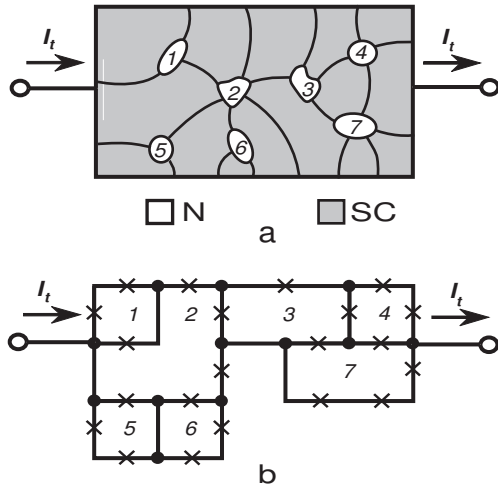


FIG. 3: Equivalent weak-link-network circuit representation of superconductor with normal-phase clusters. (a) - the percolation chart (superconducting space is shaded, weak links are shown by the curves joining together the normal-phase clusters); (b) - the electric circuit (the superconducting loops are shown by lines, the crosses on them denote weak links).

net interlaced by the superconducting loops. Each of the loops contains weak links (shown by the crosses), which join the adjacent cells and so enable the vortices to pass from one cluster to another.

Weak links form readily in HTS characterized by an extremely short coherence length.^{20,25,26} Various structural defects, which would simply cause some additional scattering at long coherence length, give rise to the weak links in HTS. On a mesoscopic scale twin boundaries are mainly responsible for weak link existence.^{27,28,29,30} Twins form especially readily in YBCO superconductors inasmuch as their unit cell is only close to the orthorhombic one. The twins can be spaced up to several nanometers apart, so even single crystal may have the fine substructure caused by twins. Magnetic and transport properties of HTS depend strongly on the orientation of twin planes with respect to the applied magnetic field.^{31,32} The flux can easily move along the weak links formed by twins.^{33,34,35,36} At last, on a macroscopic scale there are manifold structural defects which can form weak links: that may be grain or crystallite boundaries as well as barriers arising from the secondary degrading the non-stoichiometric crystal into the domains with a high and low content of oxygen.^{26,37,38,39,40} Moreover, a magnetic field further reduces a coherence length, thus resulting in more easy weak links formation.⁴¹ In conventional low-temperature superconductors weak links can be formed due to the proximity effect at the sites of minimum distance between the next normal-phase clusters.

As soon as the transport current is turned on, this one is added to all the persistent currents, maintaining the constant trapped magnetic flux. Each of these currents is

circulating through the superconducting loop around the normal-phase cluster wherein the corresponding portion of the magnetic flux is locked. The loop contains weak links that join the adjacent normal-phase clusters. As the transport current is increased, there will come a point when the overall current flowing through the weak link will exceed the critical value, so this link will switch into a resistive state. During this process the space distribution of the currents throughout the superconducting cluster is changed in such a way that the resistive subcircuit will be shunted by the superconducting paths where weak links are not damaged yet. Magnetic field created by this re-distributed transport current acts via the Lorentz force on the current circulating around the normal-phase cluster. As a result, the magnetic flux trapped therein will be forced out through the resistive weak link, which has become permeable to the vortices.

Thus, whatever the microscopic nature of weak links may be, they form the channels for vortex transport. It appears that according to their configuration each normal-phase cluster has its own value of the critical current, which contributes to the overall statistical distribution. By the critical current of the cluster we mean the current of depinning, namely, such a current at which the magnetic flux ceases to be held inside the cluster of a normal phase. When a transport current I is gradually increased, the vortices will break away first from clusters of small pinning force, and therefore, of small critical current. Thus the decrease in the trapped magnetic flux is proportional to the number of all the normal-phase clusters of critical currents less than a preset value. Therefore, the relative change in the trapped flux can be expressed with the cumulative probability function $F(I) = \Pr\{\forall I_j < I\}$ for the distribution of the critical currents of clusters:

$$\frac{\Delta\Phi}{\Phi} = F(I) \quad (2)$$

The critical current distribution $F = F(I)$ is related to the cluster area distribution $W = W(A)$, because the cluster of a larger size has more weak links over its boundary with the surrounding superconducting space, and, consequently, the smaller depinning current.

III. GEOMETRIC PROBABILITY ANALYSIS OF THE DISTRIBUTION OF WEAK LINKS OVER THE CLUSTER BOUNDARY

In order to find out the relationship between the distribution of the critical currents of the clusters and the distribution of their areas, the distribution of entry points into weak links over the boundary of a normal-phase cluster should be analyzed. We will examine the geometric properties of the normal-phase clusters in its cross-section by the plane where the transport current flows. The vortices are moving transversally to this plane so in order to leave the normal-phase cluster they have to get

over the barrier at the boundary of that cross-section. We will also suppose that the boundaries of the cluster cross-section are statistically self-similar.

The problem of exit of a vortex from a normal cluster represents the two-dimensional analogue of a problem of a random walk particle reaching a border.^{42,43} At the same time, unlike the classic problem on the distribution of the exit points, here the boundary of the area is not absorbing all over. In order to leave the cluster the vortex has to enter into one of the weak links, which are randomly arranged along the cluster perimeter. There are only discrete absorption points, which are located just at the sites where weak links are going out on the cluster boundary. In other words, these points are the points of the entry of vortices into weak links, or simply, entry points. For simplicity it will have been supposed that after the vortex reaches the entry point, it passes all the way between two adjacent normal-phase clusters without being trapped inside the weak link itself. Here the magnetic flux is transferred by Josephson vortices. The Josephson penetration depth is large enough in the considered materials, so the size of the region, where the vortex is localized, much exceeds the characteristic length of all possible structural defects that can occur along the transport channel. Thus the probability that such a vortex, driven by the Lorentz force, will be trapped in passing through a weak link is very small. This assumption agrees well with the results of research on the magnetic flux motion along weak links^{36,44,45} including twins.^{33,34,35,46,47} At the same time, it allows us to highlight the role played by the cluster boundary in the magnetic flux dynamics.

Let us consider the distribution of entry points over perimeter of a normal-phase cluster. Generally, this distribution varies from one cluster to another, so that each normal-phase cluster has the entry point distribution function $\psi(l)$ of its own, which belongs to some function class Ω . Here l is the co-ordinate measured along the cluster perimeter, so $l \in (0, P)$. In this context the functions of class Ω are random elements of the statistical distribution. The probability distribution of functions $\psi(l)$ over all the clusters can be characterized by the functional $\Pr\{\psi(l)\}$, which is equal to the probability of finding a given function $\psi(l)$.

In the most general way the geometric probability analysis of the entry point into weak link distribution can be carried out by means of path integral technique.⁴⁸ The probability that there is the function $\psi(l)$ in class Ω may be expressed by the path integral

$$\Pr\{\psi(l)|\Omega\} = \int_{(\Omega)} D\psi(l) \Pr\{\psi(l)\}$$

Therefore, the most probable function of entry point distribution is the mean over all functions of class Ω

$$\Psi(l) \equiv \overline{\psi(l)} = \int_{(\Omega)} D\psi(l) \psi(l) \Pr\{\psi(l)\} \quad (3)$$

The path integral Fourier transform on the probability functional $\Pr\{\psi(l)\}$ represents the characteristic functional

$$H[k(l)] = \frac{\int_{(\Omega)} D\psi(l) \exp\left(i \oint dl k(l) \psi(l)\right) \Pr\{\psi(l)\}}{\int_{(\Omega)} D\psi(l) \Pr\{\psi(l)\}} \quad (4)$$

where $k = k(l)$ are the functions of a reciprocal function set, and integration in the kernel $\exp\left(i \oint dl k(l) \psi(l)\right)$ is carried out over the cluster perimeter.

The characteristic functional is the path integration analog for the usual moment-generating function. The probability functional $\Pr\{\psi(l)\}$ can be written as an inverse path integral Fourier transform on the characteristic functional

$$\Pr\{\psi(l)\} = \int Dk(l) \exp\left(-i \oint dl k(l) \psi(l)\right) H[k(l)]$$

where the path integration is carried out on the reciprocal function space.

In the simplest case, when all the clusters are of equal entry point distribution, which coincides with the most probable one of Eq. (3), the probability functional $\Pr\{\psi(l)\}$ is zero for all $\psi(l)$ that differ from $\Psi(l)$, whereas $\Pr\{\Psi(l)\} = 1$. Therefore, the characteristic functional of Eq. (4) becomes

$$H[k(l)] = \exp\left(i \oint dl k(l) \Psi(l)\right) \quad (5)$$

If all entry points had fixed co-ordinates l_j instead of the random ones, their distribution would be $\psi(l) = \beta \sum_{j=1}^N \delta(l - l_j)$, where N is the number of entry points along the cluster perimeter, $\delta(l)$ is Dirac delta function. The constant β is being chosen to normalize the distribution function $\psi(l)$ to unity, so that $\beta N = 1$.

Now suppose that all the points of entries into weak links are randomly distributed with uniform probability over the cluster perimeter, so the probability to find any j -th point within some interval dl_j is proportional to its length. In that case the characteristic functional of Eq. (4) takes the form

$$\begin{aligned} H[k(l)] &= \frac{\oint \prod_{j=1}^N dl_j \exp\left(i\beta \sum_{j=1}^N \oint dl k(l) \delta(l - l_j)\right)}{\oint \prod_{j=1}^N dl_j} \\ &= \frac{1}{P^N} \oint \prod_{j=1}^N dl_j \exp\left(i\beta \sum_{j=1}^N k(l_j)\right) \\ &= \frac{1}{P^N} \prod_{j=1}^N \oint dl_j e^{i\beta k(l_j)} \end{aligned} \quad (6)$$

Expanding the function $e^{i\beta k(l)}$ in a power series at $N \gg 1$, and taking into account the condition $\beta N = 1$,

we may write

$$\frac{1}{P} \oint dl e^{i\beta k(l)} = \exp \left(i \frac{\beta}{P} \oint dl k(l) \right)$$

that, after substitution into Eq. (6), gives

$$H[k(l)] = \exp \left(i \frac{\beta N}{P} \oint dl k(l) \right) \quad (7)$$

The found characteristic functional of Eq. (7) has the form of Eq. (5) for the function of uniform distribution of entry points

$$\Psi(l) = \frac{1}{P} \quad (8)$$

This means that all the clusters have the same uniform distribution of the entry points of Eq. (8), for which the probability of finding a weak link at any point of the perimeter is independent of its position.

Let us suppose that concentration of entry points into weak links per unit perimeter length $n = \overline{N}/P$ is constant for all clusters, and all the clusters are statistically self-similar. In this case the mean number of entry points \overline{N} along the cluster perimeter is proportional to its length:

$$\overline{N} = \oint n(l) dl = nP \quad (9)$$

Next step will consist in finding the relationship between the size of a cluster and its critical current. The pinning force corresponds to such a current at which the vortices start to break away from the cluster. As the transport current is increasing, the Lorentz force, which expels the magnetic flux, increases as well. The vortices start to leave the normal-phase cluster when the Lorentz force becomes greater than the pinning force. At the same time, growing in current will result in re-distribution of the magnetic flux, which will penetrate deeper and deeper into a transition layer on that side of the surrounding superconducting space where the Lorentz force is directed (see Fig. 2(b)). In order to leave the normal-phase cluster, vortices have to reach the entry points into weak links. The exit of the magnetic flux can be considered as the result of random walks of vortices driven by the Lorentz force, which is pushing them into weak links. The similar approach has been successfully applied in analyzing the magnetic flux penetration in SQUID arrays.⁴⁴ The mean number of the entry points \overline{N} available on the cluster perimeter gives the probability measure of the number of the random walk outcomes, which are favorable for the vortex to go out. In the case of the uniform entry point distribution, from Eq. (9) it follows that $\overline{N} \propto P$, so the perimeter length also represents the probability measure of the amount of favorable outcomes for vortex to leave the cluster. The more entry points into weak links are accessible for random walk vortices, the smaller is the Lorentz force required to push the

flux out. Hence, we may write the following relation between the critical current of the cluster and its geometric size:

$$I \propto \frac{1}{\overline{N}} \propto \frac{1}{P} \quad (10)$$

This expression is true for the simplest case of uniform distribution of entry points, which is assumed to be the same for all clusters. Such a simplification allows us to emphasize that in the case being considered the magnetic flux is held in the normal-phase cluster by its boundary.

Thus, to deal with the distribution function of Eq. (1), the relation between perimeter and area of clusters should be studied. It might be natural to suppose that the perimeter-area relation obeys the well known geometric formula: $P \propto \sqrt{A}$. However, it would be a very rough approximation, because this relation holds for Euclidean geometric objects only. As was first found in Ref. 12, the boundaries of normal-phase clusters can be fractal, i.e. can have non-Euclidean features. The fractal nature of such clusters exerts an appreciable effect on the magnetic flux dynamics in superconductors.^{13,49,50}

IV. A BRIEF INTRODUCTION TO FRACTAL GEOMETRY

The notion of a fractal as an object of fractional dimension was first introduced by Mandelbrot⁵¹ in 1967 and since then it has received a lot of applications in various domains of sciences.^{52,53,54,55} This concept is closely connected to ideas of scaling and self-similarity. Self-similarity is invariance with respect to scaling; in other words, an invariance relative to multiplicative changes of scale. Whereas a usual periodicity is invariance with respect to additive translations, self-similarity is a periodicity in a logarithmic scale.

The simplest examples of self-similar objects are Cantor sets.⁵² Such a set has measure zero and, at the same time, has so many elements that it is uncountable. The Cantor set may be constructed by such a way. Let us draw a line segment, and erase its middle third. Then eliminate middle third of each remaining part, and so on. The resulting set obtained by endless erasing of the middle thirds of remaining intervals is called ‘‘Cantor dust’’.⁵² The Cantor dust forms a self-similar set because it is invariant to scaling by a factor $s = 3$. But this set is not only a self-similar one, but it is a fractal as well. Let us see what part of the set falls within one s -th part of the original set, where s is a scaling factor, and ask what fraction of the set falls into that portion? In other words, how many subsets, each is similar to the original set, are there if the length is subdivided into s parts? This number of such subsets is equal to $N = 2$, so one-half of the original set falls into one third of the initial length. The fractal dimension is defined as the logarithm of the subset number divided by the logarithm of the scaling factor: $D = \ln N / \ln s = \ln 2 / \ln 3 = 0.631$. This formula

represents the relation between the subset number and the scaling factor: $N = s^D$. Thus the fractal dimension of the Cantor dust is less than unity. This fact reflects its dust-like consistency compared to a usual line. An Euclidean line is such a set that if we change the length scale, we recover the same set of points. Hence the fractal dimension of a line coincides with the topological dimension, and both of them are equal to unity. Generally, a fractal object has a fractional dimension. A fractal set is such a set for which the fractal dimension strictly exceeds its topological dimension.⁵³

The Cantor dust gives an example of determinate fractal that is self-similar by deterministic construction. But the same approach can be applied to the stochastic fractals, which are statistically self-similar.⁵⁴ The fundamental feature of any fractals, both determinate and the stochastic ones, is that its characteristic measures obey a scaling law that includes an exponent called the fractal dimension.

Fractal dimension of statistically self-similar curve can be estimated by covering the curve by square grid. The size of the grid cell $L \times L$ should be small enough for measuring all the bend of the curve. If the whole curve (the boundary of the normal-phase cluster cross-section) goes in square of side L_{\max} , then each of $N(L)$ self-similar subsets of that curve will go in square of side $L = L_{\max}/s$, where s is scaling factor. Let us suppose that the curve is self-similar at any scaling factor. The minimum number of such squares of side L needed to cover the explored curve is equal to

$$N(L) = s^D = \left(\frac{L_{\max}}{L}\right)^D \propto L^{-D}$$

where D is the fractal dimension of the curve (so-called coastline dimension).⁵² So we have the formula that determines the fractal dimension

$$D = \frac{\ln N(L)}{\ln(L_{\max}/L)} \quad (11)$$

It is obvious that the magnitude of D is always below the topological dimension of a plane, which is equal to two.

The ratio between the size of measuring cell L and the big square side L_{\max} sets the unit of measurement of length. At $L_{\max} = 1$ the expression for the fractal dimension of Eq. (11) takes the form $D = -\ln(N(L))/\ln(L)$.

Thus, in order to find the fractal dimension it is necessary to count the total number $N(L)$ of non-empty cells of area L^2 , which cover the curve. To attain the highest precision of estimate we have to get wide range of L and to average obtained values of D over all the configurations.

The length of topologically one-dimensional fractal curve of size L_{\max} , measured with an accuracy of L , is equal to a product of the number of cells, which cover that curve, and the linear size of the measuring cell

$$P = NL = \left(\frac{L_{\max}}{L}\right)^D L = \frac{L_{\max}^D}{L^{D-1}} \quad (12)$$

In other words, if the whole curve goes in the scale of length L_{\max} , then in the smaller scale of $L = L_{\max}/s$ (i. e. for the yardstick of a smaller size) the same curve will consist of $N = s^D$ pieces of length L . As is seen from the formula of Eq. (12), the length of a fractal curve is not well defined, because its value depends on the accuracy of the measurements, and even diverges as the yardstick size L is reduced infinitely. At the same time, the area restricted by any closed (including fractal) curve is well-defined finite quantity, which is proportional to its squared linear size: $A \propto L_{\max}^2$. According to expression of Eq. (12), the length of the perimeter of the figure, formed by the closed fractal curve, is proportional to its linear size raised to a power of fractal dimension: $P \propto L_{\max}^D$. Hence it follows that the perimeter of fractal figure and enclosed area have to obey a scaling law

$$P^{1/D} \propto A^{1/2} \quad (13)$$

The perimeter-area scaling law of Eq. (13) expresses the generalized Euclid theorem about measures of similar figures, stating that the ratios of corresponding measures are equal when reduced to the same dimension.⁵³ This assertion is valid both for Euclidean figures and for the fractal ones.

The fractal approach has been found to be most useful in an investigation of inhomogeneous materials. There are many possibilities both the determinate fractals and the stochastic ones to be formed in composite superconductors. As an example of the first kind the multi-layered structures prepared by electron-beam deposition of superconductor (Nb) and normal metal (Cu) layers with fractal stacking sequence on sapphire substrates can be mentioned.⁵⁶ In order to obtain stochastic fractal clusters, it is essential that the process like the diffusion-limited aggregation would take place in the course of the synthesis of material.⁵⁵ The similar process can be realized, for instance, when thin films are evaporated. So, in Ref. 57 the films of fractal structure has been grown by vapor deposition of gold on silicon substrate with silicon nitride buffer sub-layer. It is worthy of note that porous, random, or highly ramified clusters do not necessarily all are fractals. A fractal cluster has such a property that its characteristic measures (in what follows - the perimeter and the enclosed area) have to obey the certain scaling law that includes an exponent named fractal dimension.^{52,55}

The fractal clusters can be also formed in such highly inhomogeneous materials as high-temperature superconductors. So, the fractal dissipative regime has been observed in high-resolution measurements of dynamical resistance of BSCCO and BPSCCO composites containing normal-phase inclusions of Ag.¹¹ The fractal properties of the normal-phase clusters contained in YBCO films, which were prepared by magnetron sputtering on sapphire substrate with a cerium oxide buffer sub-layer, have been found in Ref. 12. Percolation clusters are another example of fractals in superconductors.^{58,59} Although,

mathematically, the percolation cluster is a fractal at the threshold point only, the fractal approach works well for any clusters which have a scaling feature.^{60,61,62} In that case the normal-phase clusters may be formed by inclusions of different chemical composition, as well as the domains of reduced superconducting order parameter can act as such clusters. The existence of the fractal inclusions of this kind can be demonstrated by the fractal dissipation, which has been observed in non-textured polycrystalline YBCO and GdBCO bulk samples.¹¹ The fractal structure of clusters near the percolation threshold in epitaxial YBCO films has been fully considered in Ref. 63. Of special interest are the works of Refs. 10,64, where the fractal penetration of magnetic flux in thin HTS films has been investigated by magneto-optical technique. Epitaxial TlBCO films were grown by magnetron sputtering on SrTiO₃ substrates, and YBCO films were prepared by pulsed laser deposition on NdGaO₃ substrates. The cluster structure of such films is clearly visible on the Atomic Force Microscopy picture published in Ref. 10, whereas the magnetic flux, penetrating into the sample from the outside, has well-definite fractal front.

V. FRACTAL GEOMETRY OF NORMAL-PHASE CLUSTERS

The scaling law of Eq. (13) furnishes a clue to find relation between the critical current of the cluster and its geometric size. Using the formula of Eq. (10), which links the cluster size and its current of depinning, can we get the following expression: $I = \alpha A^{-D/2}$, where α is the form factor, and D is the fractal dimension of the cluster boundary. In the general way the cluster area distribution can be described by gamma distribution, which is appropriate for the most part of practically realizable cases.^{49,50,65,66} This distribution is characterized by the following cumulative probability function:

$$W(A) = (\Gamma(g+1))^{-1} \gamma\left(g+1, \frac{A}{A_0}\right) \quad (14)$$

where $\Gamma(\nu)$ is Euler gamma function, $\gamma(\nu)$ is the incomplete gamma function, A_0 and g are the parameters of gamma distribution that control the mean area of the cluster $\bar{A} = (g+1)A_0$ and its variance $\sigma_A^2 = (g+1)A_0^2$.

In accordance with starting formulas of Eq. (1) and Eq. (2), gamma distribution of cluster areas of Eq. (14) gives rise to the critical current distribution of the form:

$$F(i) = (\Gamma(g+1))^{-1} \Gamma\left(g+1, Gi^{-2/D}\right) \quad (15)$$

where $G \equiv (\theta^\theta / (\theta^{g+1} - (D/2) \exp(\theta) \Gamma(g+1, \theta)))^{2/D}$, $\theta \equiv g+1+D/2$, $\Gamma(\nu, z)$ is the complementary incomplete gamma function, $i = I/I_c$ is the dimensionless electric current, $I_c = \alpha(A_0 G)^{-D/2}$ is the critical current of the transition into a resistive state. The found cumulative probability function of Eq. (15) allows to derive the

probability density $f(i) \equiv dF/di$ for the critical current distribution:

$$f(i) = \frac{2G^{g+1}}{D\Gamma(g+1)} i^{-(2/D)(g+1)-1} \exp\left(-Gi^{-2/D}\right) \quad (16)$$

This distribution allows us to fully describe the effect of the transport current on the trapped magnetic flux taking into account the fractal properties of the normal-phase clusters. Let us note that the probability density for the critical current distribution of Eq. (16) is equal to zero at $i = 0$, which implies the absence of any contribution from negative and zero currents. This will allow us to avoid any artificial assumption about the existence of a vortex liquid, having finite resistance in the absence of transport currents due to the presence of free vortices: $r(i \rightarrow 0) \neq 0$. Such an assumption is made, for example, in the case of normal distribution of critical currents.⁶⁷

In order to clear up how the developed approach can be used in practice, the geometric probability analysis of electron photomicrographs of superconducting films was carried out. For this purpose electron photomicrographs of YBCO film prepared by magnetron sputtering on sapphire substrate with a cerium oxide buffer sub-layer have been scanned. The normal phase has occupied 20% of the total surface only, so the transport current can flow through the sufficiently dense percolation superconducting cluster. The perimeters and areas of clusters have been measured by covering their digitized pictures with a square grid of spacing $60 \times 60 \text{ nm}^2$. The results of the statistical treatment of these data are presented in Fig. 4. The primary sampling has contained 528 normal-phase clusters located on the scanned region of a total area of $200 \mu\text{m}^2$. The distribution of the cluster areas is fitted well to exponential cumulative probability function, as is shown on the histogram in the lower inset of Fig. 4. The number of clusters that fall within the assigned rank is plotted on the ordinate of this graph; the rank number is plotted on the abscissa. A high skewness (1.765) as well as the statistically insignificant (5%) difference between the sample mean area of the cluster and the standard deviation also attests that there an exponential distribution of the cluster areas holds true. This distribution is a special case of gamma distribution for which $g = 0$, so the cumulative probability function of Eq. (14) can be simplified to the following form:

$$W(A) = 1 - \exp\left(-\frac{A}{\bar{A}}\right) \quad (17)$$

The exponential distribution has only one characteristic parameter - the mean cluster area \bar{A} .

The obtained data allow us to find the perimeter-area relation for the normal-phase clusters. All the points in Fig. 4 fall on a straight line in double logarithmic scale with correlation coefficient of 0.929. Accordingly to the scaling relation of Eq. (13), the slope of the regression line gives the estimate of fractal dimension of the cluster perimeter, which is equal to $D = 1.44 \pm 0.02$. The graph

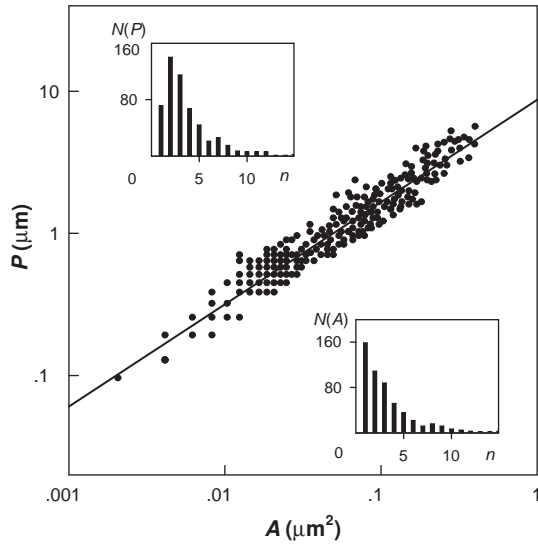


FIG. 4: Perimeter-area relationship for the normal-phase clusters with fractal boundary. The chart is built for the primary sampling containing 528 normal-phase clusters. The insets represent histograms of sampling for corresponding distributions.

in Fig. 4 shows that the scaling law for perimeter and area, which is inherent to fractals, is valid in the range of almost three orders of magnitude in cluster area. The perimeter-area scaling behavior means that there is no characteristic length scale in the range of two orders of linear size of the normal-phase cluster. Whatever the shape and size of the clusters may be, all the points fall closely on the same straight line in logarithmic scale; so that there are no apparent kinks or bends on the graph. This point that the found value of the fractal dimension differs appreciably from unity engages a great attention. What this means is that the fractal properties of the cluster boundary are of prime importance here.

The geometric probability properties of the normal-phase clusters are responsible for main features of the critical current statistical distribution. Now, knowing the fractal dimension of the cluster boundaries, the change in the trapped magnetic flux caused by the transport current can be found with aid of Eq. (2). The exponential distribution of the cluster areas of Eq. (17) gives rise to the exponential-hyperbolic distribution of critical currents

$$F(i) = \exp \left(- \left(\frac{2+D}{2} \right)^{2/D+1} i^{-2/D} \right) \quad (18)$$

which follows from Eq. (15) at $g = 0$. The effect of a transport current on the trapped magnetic flux is illustrated in Fig. 5 for the case of Euclidean clusters (dotted curve), and for the clusters of found fractal dimension $D = 1.44$ (solid curve).

In order to get the relationship between the dynamics of the trapped magnetic flux and the geometric properties

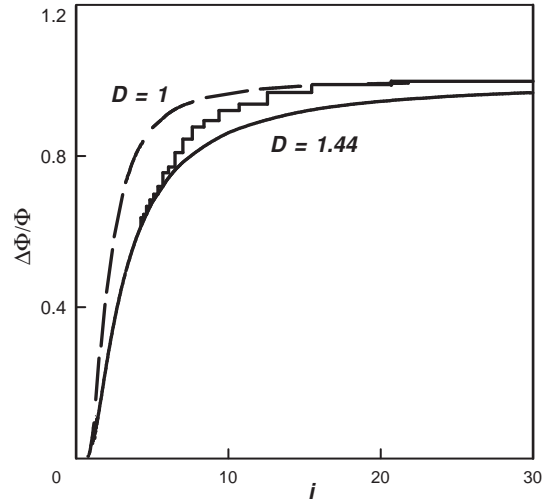


FIG. 5: Crossover between the fractal and Euclidean regimes on dependence of the magnetic flux trapped in fractal clusters of a normal phase on a transport current. The solid line shows the decrease in trapped flux for the fractal clusters of boundary dimension $D = 1.44$; the dotted line corresponds to the case of Euclidean clusters ($D = 1$); step line is the sample empirical function of critical current distribution.

of the superconducting structure the empirical function of the distribution of the critical currents $F^* = F^*(i)$ has been found. First, the empirical distribution function $W^* = W^*(A)$ for the sampling of the areas of the normal-phase clusters has been obtained. The value of $W^*(A)$ was calculated for each order statistic as the relative number of clusters of area smaller than a given value A . Next, the empirical distribution of the critical currents was computed for the same order statistics using the formulas:

$$\left. \begin{aligned} F^* &= 1 - W^* \\ i &= ((2+D)/2)^{(2+D)/2} (\bar{A}/A)^{D/2} \end{aligned} \right\}$$

This function, shown in Fig. 5 by the step line, gives a statistical estimate of the cumulative probability function of Eq. (18). As is seen from this figure, both distributions coincide well in the range of currents $i < 6$. Starting with the value of the current $i = 6$ the crossover from the fractal regime to the Euclidean one is observed. This transition into the Euclidean regime is over at large transport currents, when the magnetic flux changes mainly for the breaking of the vortices away from the small clusters (as the smaller clusters have the larger pinning force). The observed crossover has its origin in the finite resolution capability of measuring the cluster sizes. When estimating the fractal dimension, we have to take into account that the resolution of the measurement of any geometric sizes is finite. The peculiarity of the topologically one-dimensional fractal curve is that its measured length depends on the measurement accuracy.⁵² In our case such a fractal curve is represented by the boundary of the normal-phase cluster. That is why just the statis-

tical distribution of the cluster areas, rather than their perimeters, is fundamental for finding the critical current distribution. The topological dimension of perimeter is equal to unity and does not coincide with its fractal dimension, which strictly exceeds the unity. Therefore the perimeter length of a fractal cluster is not well defined, because its value depends on the yardstick size. On the other hand, the topological dimension of the cluster area is the same as the fractal one (both are equal to two). Thus, the area restricted by the fractal curve is a well-defined quantity.

Taking into account the finite resolution effect, the perimeter-area relationship of Eq. (13) can be re-written in the following form

$$P(\delta) \propto \delta^{1-D} (A(\delta))^{D/2} \quad (19)$$

where δ is the yardstick size used to measure this length, $(1 - D)$ is the Hausdorff codimension for the Euclidean one-dimensional space. This relation holds true when the yardstick length is small enough to measure accurately the boundary of all smallest clusters in sampling. When the resolution is deficient, the Euclidean part of the perimeter length will dominate the fractal one, so there is no way to find the fractal dimension using the scaling relation of Eq. (19). It means that if the length of a fractal curve was measured too roughly with the very large yardstick, its fractal properties could not be detected, and therefore such a geometrical object would be manifested itself as Euclidean one. It is just the resolution deficiency occurs at the crossover point in Fig. 5. Starting with the cluster area less than some value (which corresponds to the currents of $i > 6$) it is impossible to measure all “skerries” and “fjords” on the cluster coastlines, whereas all the clusters of area less than the size of the measuring cell (3600 nm^2 that relates to the currents of $i > 23$), exhibit themselves as objects of Euclidean boundaries. This resolution deficiency can be also observed in Fig. 4: some points at its lower left corner are arranged discretely with the spacing equal to the limit of resolution (60 nm), because some marks for smallest clusters coincide for the finite resolution of the picture digitization procedure.

The fractal dimension was found above by means of regression analysis of the whole primary sampling, where the very small clusters of sizes lying at the breaking point of the resolution limit were also included. In order to evaluate how the finite resolution affects the accuracy of the estimation of the fractal dimension, all the points, for which the resolution deficiency was observed, were eliminated from the primary sampling. So the truncated sampling has been formed in such a way that only 380 clusters, for which the resolution deficiency is not appeared yet, have been selected from the primary sampling. The regression analysis of the truncated sampling is presented in Fig. 6. The least squares treatment of perimeter-area data gives the adjusted magnitude of the fractal dimension: $D = 1.47 \pm 0.03$. The found value virtually does not differ from the previous one within the

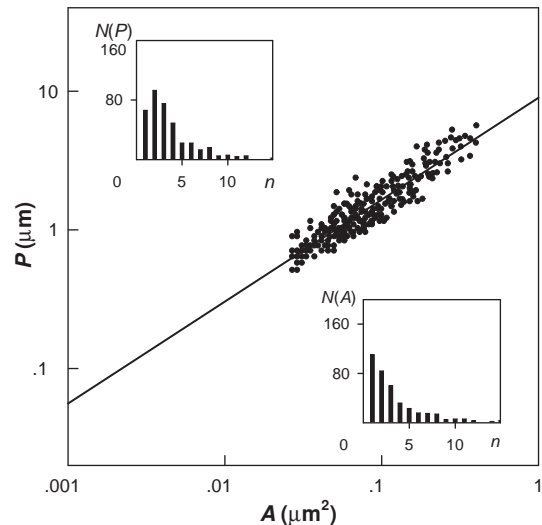


FIG. 6: Perimeter-area relationship for the normal-phase clusters with fractal boundary. The chart is built for the truncated sampling containing 380 normal-phase clusters. The insets represent histograms of sampling for corresponding distributions.

accuracy of the statistical estimation, whereas the correlation coefficient (which becomes equal to 0.869) falls by six hundredth only. Therefore, we can conclude that the found estimate of the fractal dimension is robust.

VI. THE PINNING GAIN FOR THE MAGNETIC FLUX TRAPPED IN FRACTAL CLUSTERS OF A NORMAL PHASE

It has been revealed that the fractality of the cluster boundaries intensifies the pinning. As can be seen from Fig. 7, the decrease in the trapped magnetic flux at the same value of the transport current is less for larger fractal dimension. The relative change in the trapped flux $\Delta\Phi/\Phi$, which, according to formula of Eq. (2), can be calculated from Eq. (18), defines the density of vortices n broken away from the pinning centers by the current i :

$$n(i) = \frac{B}{\Phi_0} \int_0^i f(i') di' = \frac{B}{\Phi_0} \frac{\Delta\Phi}{\Phi} \quad (20)$$

where B is the magnetic field, $\Phi_0 \equiv hc/(2e)$ is the magnetic flux quantum (h is Planck's constant, c is the velocity of light, e is the electron charge). The graph of the change in the trapped flux as a function of transport current, shown in Fig. 7, coincides qualitatively with the curves obtained in experiments on the magnetization of YBCO films subjected to current pulses.^{68,69} Figure 7 also displays such an important property of superconducting structure containing fractal clusters of a normal phase: the fractality intensifies the magnetic flux trapping, hindering its breaking away from pinning centers,

and thereby enhances the critical current which sample is capable to withstand, remaining in a superconducting state. The pinning amplification can be characterized by the pinning gain factor

$$k_\Phi \equiv 20 \log_{10} \frac{\Delta\Phi(D=1)}{\Delta\Phi(\text{current value of } D)}, \quad \text{dB} \quad (21)$$

which is equal to relative decrease in the fraction of magnetic flux broken away from fractal clusters of fractal dimension D compared to the case of Euclidean ones. Dependencies of the pinning gain on the transport current for different fractal dimension at $g = 0$ are shown in the inset of Fig. 7. The highest amplification (about 10 dB) is reached when the cluster boundaries have the greatest possible fractality. Figure 7 demonstrates that with increase in fractal dimension the trapped magnetic flux is changed less and less by the action of the transport current. The pinning gain of Eq. (21) characterizes the properties of a superconductor in the range of the transport currents corresponding to a resistive state ($i > 1$). At smaller current the total trapped flux remains nearly unchanged (see Fig. 7) for lack of pinning centers of such small critical currents, so the breaking of the vortices away has not started yet. When the vortices start to leave the normal-phase clusters and move through the weak links, their motion induces an electric field, which, in turn, creates the voltage drop across the sample. Therefore, the passage of electric current is accompanied by the energy dissipation. As for any hard superconductor (that is to say, type-II, with pinning centers) this dissipation does not mean the destruction of phase coherence yet. Some dissipation always accompanies any motion of a magnetic flux that can happen in a hard superconductor even at low transport current. Therefore the critical current in such materials cannot be specified as the greatest non-dissipative current. Superconducting state collapses only when a growth of dissipation becomes avalanche-like as a result of thermo-magnetic instability.

The principal reason of pinning enhancement due to the fractality of the normal-phase clusters lies in the fundamental properties of the critical current distribution. Figure 8 demonstrates the peculiarities of the fractal probability density specified by Eq. (18). As may be seen from this graph, the bell-shaped curve of the distribution broadens out, moving towards greater magnitudes of current as the fractal dimension increases. It means that more and more of the small clusters, which can trap the vortices best, are being involved in the game. Hence the number of vortices broken away from pinning centers by the Lorentz force is reducing, so the smaller part of a magnetic flux can flow. The shift of the critical current distribution towards higher currents can be described by dependencies of the mean critical current distribution on the fractal dimension, as it is shown in the inset of Fig. 8. The mean critical current obeys the strong super-linear law specified by Euler gamma function:

$$\bar{i} = \left(\frac{2+D}{2} \right)^{(2+D)/2} \Gamma \left(1 - \frac{D}{2} \right) \quad (22)$$

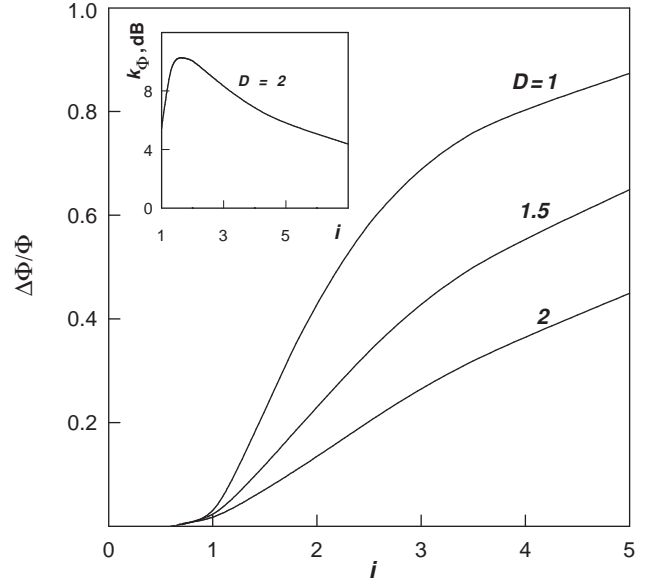


FIG. 7: Effect of a transport current on the magnetic flux trapped in fractal clusters of a normal phase. The inset shows the pinning gain for the different fractal dimension of the cluster boundary.

Figure 8 clearly demonstrates that increasing the fractal dimension gives a growth of the contribution made by clusters of greater critical current to the overall distribution, resulting just in enhancement of the magnetic flux trapping.

VII. ANOMALOUS STATISTICAL PROPERTIES OF THE CRITICAL CURRENT FRACTAL DISTRIBUTION

In the general case of gamma-distribution of the normal-phase cluster areas of Eq. (14) the probability density for the cluster areas has the form

$$w(A) = \frac{A^g \exp(-A/A_0)}{\Gamma(g+1) A_0^{g+1}} \quad (23)$$

For further consideration it is convenient to introduce the dimensionless area of the cluster \tilde{a} , for which the distribution function of Eq. (23) can be rewritten as:

$$w(\tilde{a}) = \frac{(g+1)^{g+1}}{\Gamma(g+1)} \tilde{a}^g \exp(-(g+1)\tilde{a}) \quad (24)$$

The mean dimensionless area of the cluster is equal to unity, whereas the variance is determined by one parameter only: $\sigma_a^2 = 1/(g+1)$. The critical current distribution has the exponential-hyperbolic form of Eq. (16), for which the mean critical current, instead of Eq. (22), is

$$\bar{i} = G^{\frac{D}{2}} \frac{\Gamma(g+1-D/2)}{\Gamma(g+1)} \quad (25)$$

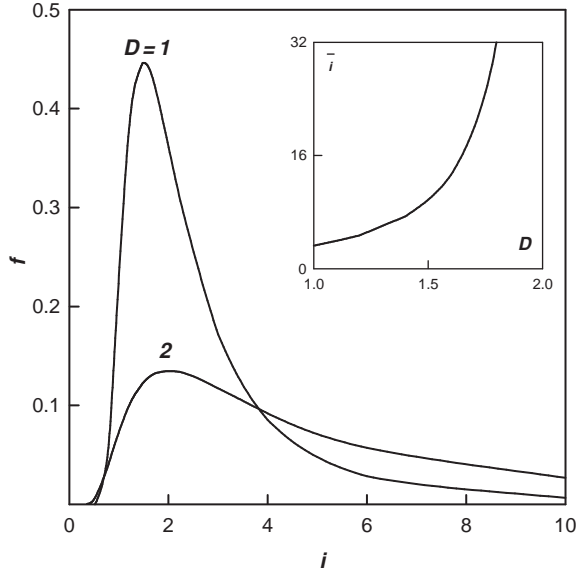


FIG. 8: Influence of the fractal dimension of the boundary of the normal-phase clusters on the critical current distribution. The inset shows the dependencies of the mean critical current on the fractal dimension.

The critical current distribution has the skew bell-shaped form with inherent broad “tail” extended over the region of high currents (see Fig. 8). The mean critical current of Eq. (25), just as mean current of Eq. (22) in the special case of exponential distribution of the normal-phase clusters areas, is divergent in the range of fractal dimensions $D \geq 2(g+1)$.

The gamma distribution of the critical currents of Eq. (16) spreads out with some shift to the right as g -parameter decreases. This broadening can be characterized by the standard deviation of critical currents

$$\sigma_i = G^{\frac{D}{2}} \sqrt{\frac{\Gamma(g+1-D)}{\Gamma(g+1)} - \left(\frac{\Gamma(g+1-D/2)}{\Gamma(g+1)} \right)^2} \quad (26)$$

The standard deviation grows nonlinearly with increase in the fractal dimension. The peculiarity of the distribution of Eq. (16) is that its variance becomes infinite in the range of fractal dimensions $D \geq g+1$. At the same time, the mode of the distribution $\text{mode} f(i) = (G/\theta)^{D/2}$ remains finite for all possible values of the fractal dimension $1 \leq D \leq 2$. The distributions with divergent variance are known in probability theory - the classic example of that kind is Cauchy distribution.⁷⁰ However, such an anomalous feature of exponential-hyperbolic distribution of Eq. (16) is of special interest, inasmuch as the current-carrying capability of a superconductor would be expected to increase in the region of giant variance. Then the statistical distribution of critical currents has a very elongated “tail” containing the contributions from the clusters of the highest depinning currents.

The reason for divergence of statistical moments of

the exponential-hyperbolic critical current distribution of Eq. (16) consists in the behavior of the cluster area distribution of Eq. (24). The form of this function takes essentially different shapes depending on the sign of g -parameter - from the skew unimodal curve at $g > 0$ to the monotonic curve with hyperbolic singularity at zero point at $g < 0$. In the borderline case of $g = 0$, which separates these different kinds of the functions, the distribution obeys an exponential law. It is just for negative values of g -parameter that the mean critical current diverges. The contribution from the clusters of small area to the overall distribution grows at $g < 0$. Since the clusters of small size have the least number of weak links over a perimeter, they can best trap the magnetic flux. Therefore, an increase of the part of small clusters in the area distribution of Eq. (24) leads to a growth of the contribution with high depinning currents made by these clusters in the critical current distribution of Eq. (16). Just as a result of this feature the mean critical current diverges at $g < 0$. Nevertheless, the total area between the curve of the probability density and the abscissa remains finite by virtue of the normalization requirement.

Obviously, the proper critical current cannot be infinitely high as well as the clusters of infinitesimal area do not really exist. There is the minimum value of the normal-phase cluster area A_m , which is limited by the processes of the film growth. So in YBCO based composites prepared by magnetron sputtering,¹² the sample value of minimum area of the normal-phase cluster has been equal to $A_m = 2070 \text{ nm}^2$ at mean cluster area $\bar{A} = 76500 \text{ nm}^2$, that corresponds to the lower bound of the dimensionless area of the cluster $a_m \equiv A_m/\bar{A} = 0.027$. In view of this limitation, we will describe the distribution of the normal-phase cluster areas by the truncated version of the probability density of Eq. (24):

$$w(a | a \geq a_m) = \frac{h(a - a_m)}{1 - W(a_m)} w(a) \quad (27)$$

where $h(x) \equiv \begin{cases} 1 & \text{for } x \geq 0 \\ 0 & \text{for } x < 0 \end{cases}$ is the Heaviside step function, and

$$W(a_m) \equiv \int_0^{a_m} w(a) da = \frac{\gamma(g+1, (g+1)a_m)}{\Gamma(g+1)} \quad (28)$$

is the truncation degree, which is equal to the probability $\Pr\{\forall a < a_m\}$ to find the cluster of area smaller than the least possible value a_m in the initial population. In the expression of Eq. (28) $\gamma(\nu, z)$ is the complementary gamma function.

The expression of Eq. (27) gives the conditional distribution of probability, for which all the events of finding a cluster of area less than a_m are excluded. Thus the truncation provides a natural way to fulfil our initial assumption that the cluster size has to be greater than the coherence and penetration lengths. New distribution of cluster areas gives rise to the truncated distribution of

the critical currents:

$$f(i|i \leq i_m) = \frac{h(i_m - i)}{1 - W(a_m)} f(i) \quad (29)$$

where $i_m \equiv (G/(g+1)a_m)^{D/2}$ is the upper bound of the depinning current, which corresponds to the cluster of the least possible area a_m .

Then, instead of Eqs. (26) and (25), the standard deviation and mean critical current are

$$\sigma_i^* = G^{\frac{D}{2}} \sqrt{\frac{\Gamma(g+1-D, (g+1)a_m)}{\Gamma(g+1, (g+1)a_m)}} - \left(\frac{\Gamma(g+1-D/2, (g+1)a_m)}{\Gamma(g+1, (g+1)a_m)} \right)^2 \quad (30)$$

$$\bar{i}^* = G^{\frac{D}{2}} \frac{\Gamma(g+1-D/2, (g+1)a_m)}{\Gamma(g+1, (g+1)a_m)} \quad (31)$$

For the truncated distribution of Eq. (29) the possible values of depinning currents are bounded from above by the quantity i_m , therefore the mean critical current as well as the variance do not diverge any more. Both of these characteristics are finite for any fractal dimensions, including the case of maximum fractality ($D = 2$). The truncation degree is related to the least possible area of the cluster by the equation (28).

The degree of truncation gives the probability measure of the number of normal-phase clusters that have the area smaller than the lower bound a_m in the initial distribution. If the magnitude of $W(a_m)$ is sufficiently small (no more than several percent), then the procedure of truncation scarcely affects the initial shape of the distribution and still enables the contribution from the clusters of zero area (therefore, of infinitely high depinning current) to be eliminated. It is interesting to note that the very similar situation occurs in analyzing the statistics of the areas of fractal islands in the ocean.⁵³ The island areas obey the Pareto distribution, which also has the hyperbolic singularity at zero point that causes certain of its moments to diverge. For exponential distribution of the cluster areas, which is valid in the above-mentioned case of YBCO films,¹² the probability to find the cluster of area smaller than a_m in the sampling is equal to $\Pr\{\forall a < a_m\} = 2.7\%$ only. In principle, the truncation procedure could be made here, too, but there is no need for that, because the contribution of infinitesimally small clusters is finite at $g = 0$ (and equal to zero at $g > 0$).

As the fractal dimension increases, the critical current distribution broadens out (the variance grows), moving towards higher currents (the mean critical current grows, too). This trend is further enhanced with decreasing g -parameter. The most current-carrying capability of a superconductor should be achieved when the clusters of small size, which have the highest currents of depinning, contribute maximally to the overall distribution of the critical currents. Such a situation takes place just in the

region of giant variance of critical currents. So far, the least magnitude of g -parameter (equal to zero) has been realized in YBCO composites containing normal-phase clusters of fractal dimension $D = 1.44$.¹² The critical currents of superconducting films with such clusters are higher than usual.^{8,68,69} It would thus be expected to further improve the current-carrying capability in superconductors containing normal-phase clusters, which will be characterized by area distribution with negative magnitudes of g -parameter, especially at the most values of fractal dimensions.

VIII. CURRENT-VOLTAGE CHARACTERISTICS AND VORTEX DYNAMICS NEAR THE RESISTIVE TRANSITION

By virtue of the fact that any motion of the magnetic flux causes the energy dissipation in superconductors, the question of how such a process could be prevented, or only suppressed, is of prime practical importance. The study of resistive state peculiarities leads to the conclusion that the cluster fractality exerts influence on the electric field induced by the flux motion. The found distribution of the critical currents allows us to find the electric field arising from the magnetic flux motion after the vortices have been broken away from the pinning centers. Inasmuch as each normal-phase cluster contributes to the total critical current distribution, the voltage V across a superconductor can be represented as the response to the sum of effects made by the contribution from each cluster. Such a response can be expressed as a convolution integral

$$\frac{v}{r_f} = \int_0^i (i - i') f(i') di' \quad (32)$$

where r_f is the dimensionless flux flow resistance. The similar approach is used universally in all the cases where the distribution of the depinning currents takes place.^{67,71,72} The subsequent consideration will be essentially concentrated on the consequences of the fractal nature of the normal-phase clusters specified by the distribution of Eqs. (15), (18), so all the problems related to possible dependence of the flux flow resistance r_f on a transport current will not be taken up here. The voltage across a superconductor V and flux flow resistance R_f are related to the corresponding dimensionless quantities v and r_f by the relationship: $V/R_f = I_c(v/r_f)$.

After substitution of the critical current distribution of Eq. (16) into the expression of Eq. (32), upon integration, we get the final expression for the current-voltage (V - I) characteristics in the general case of the gamma-distribution of the cluster areas:

$$\frac{v}{r_f} = \frac{1}{\Gamma(g+1)} \left(i\Gamma\left(g+1, Gi^{-2/D}\right) - G^{D/2}\Gamma\left(g+1 - \frac{D}{2}, Gi^{-2/D}\right) \right) \quad (33)$$

In the special case of exponential cluster area distribution ($g=0$) the general formula of Eq. (33) can be simplified:

$$\frac{v}{r_f} = i \exp\left(-Ci^{-2/D}\right) - C^{D/2}\Gamma\left(1 - \frac{D}{2}, Ci^{-2/D}\right) \quad (34)$$

where $C \equiv ((2+D)/2)^{2/D+1}$.

In extreme cases of Euclidean clusters and clusters of the most fractality the expression of Eq. (34) can be further transformed:

(i) Clusters of Euclidean boundary ($D = 1$ at $g = 0$):

$$\frac{v}{r_f} = i \exp\left(-\frac{3.375}{i^2}\right) - \sqrt{3.375\pi} \operatorname{erfc}\left(\frac{\sqrt{3.375}}{i}\right) \quad (35)$$

where $\operatorname{erfc}(z)$ is the complementary error function.

(ii) Clusters of boundary with the maximum fractality ($D = 2$ at $g = 0$):

$$\frac{v}{r_f} = i \exp\left(-\frac{4}{i}\right) + 4 \operatorname{Ei}\left(-\frac{4}{i}\right) \quad (36)$$

where $\operatorname{Ei}(z)$ is the exponential integral function.

The V - I characteristics calculated using the formulas of Eqs. (34) - (36) are presented in Fig. 9. Two lines drawn for extreme case of $D = 1$ and $D = 2$ bound the region the V - I characteristics can fall within for any possible values of fractal dimension. Figure 9 shows that the fractality reduces appreciably an electric field arising from the magnetic flux motion. This effect is especially strong in this range of the currents ($1 < i < 3$), where the pinning enhancement also has a maximum (see also Fig. 7). Both these effects have the same nature, inasmuch as their reason lies in the peculiarities of the critical current distribution. The influence of the fractal dimension of the cluster boundary on the critical current distribution is demonstrated in Fig. 8. An increase of fractality causes a significant broadening of the tail of the distribution $f = f(i)$. Therefore, more of small clusters, which have higher critical currents of depinning, are being involved in the process. Hence the smaller number of vortices can move, creating the smaller electric field. In turn, the smaller the electric field is, the smaller is the energy dissipated when the transport current passes through the sample. Therefore, the decrease in heat-evolution, which could cause transition of a superconductor into a normal state, means that the current-carrying capability of a superconductor containing such fractal clusters is enhanced.

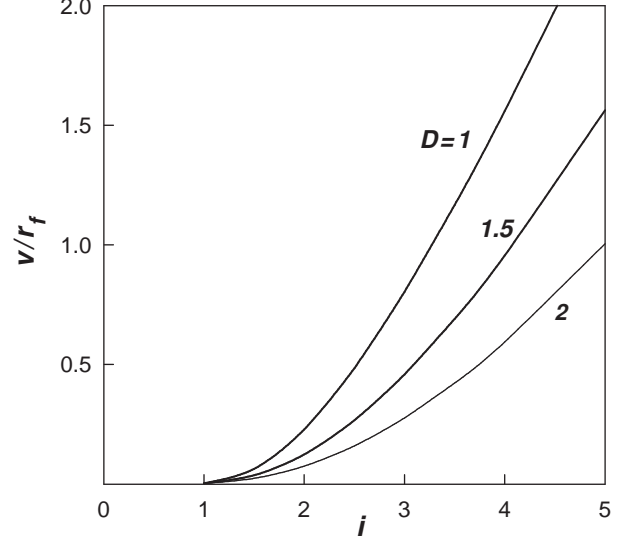


FIG. 9: Current-voltage characteristics of superconductors with fractal clusters of a normal phase.

Though the fractality of the clusters reduces the voltage arising from the vortex motion in the range of the currents $i > 1$, the situation is quite different in the neighborhood of the resistive transition below the critical current. When $i < 1$, the higher the fractal dimension of the normal-phase cluster is, the larger is the voltage across a sample and the more stretched is the region of initial dissipation in V - I characteristic. The critical current i_c is preceded by some initial region of the finite voltage drop starting with i_{on} , so the resistive transition is not absolutely abrupt. The existence of this initial section on the V - I characteristic arises from the peculiarities of the fractal distribution in the range of small currents. It has been just a similar initial region of fractal dissipation has been observed in high-resolution measurements of dynamical resistance of HTS-normal metal composites.¹¹

The significant difference in V - I characteristic behavior below and above the resistive transition is related to dependence of free vortex density on the fractal dimension for various transport currents. The resistive characteristics provide additional information about the nature of a vortex state in superconductor with fractal clusters of a normal phase. Since the V - I characteristics of Eqs. (33) - (34) are non-linear, dc (static) resistance is not constant and depends on the transport current. The more convenient parameter is the differential resistance $r_d = dv/di$, a small-signal ac parameter that gives the slope of the V - I characteristic. The corresponding dimensional quantity R_d can be found using the formulas $R_d = r_d R_f / r_f$. Figure 10 shows the graphs of the differential resistance as a function of transport current for superconductor with fractal normal-phase clusters. The curves drawn for the

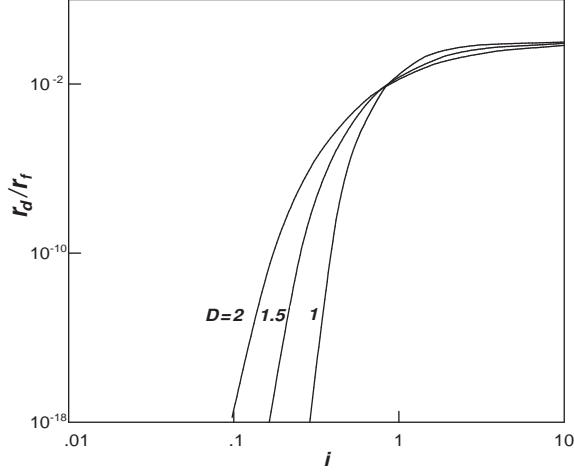


FIG. 10: Dependence of the dc resistance on the transport current for superconductor with fractal normal-phase clusters. The dashed horizontal line $r = r_f$ at the upper right corresponds to the viscous flow of a magnetic flux.

Euclidean clusters ($D = 1$) and for the clusters of the most fractal boundaries ($D = 2$) bound a region containing all the resistive characteristics for an arbitrary fractal dimension. As an example, the dashed curve shows the case of the fractal dimension $D = 1.5$. The dependencies of resistance on the current shown in Fig. 10 are typical of the vortex glass, inasmuch as the curves plotted on a double logarithmic scale are convex and the resistance tends to zero as the transport current decreases, $r_d(i \rightarrow 0) \rightarrow 0$, which is related to the flux creep suppression.^{20,67} A vortex glass represents an ordered system of vortices without any long-range ordering. At the same time, the vortex configuration is stable in time and can be characterized by the order parameter of the glassy state.^{73,74} In the H - T phase diagram, mixed state of the vortex glass type exists in the region below the irreversibility line. The dashed horizontal line at the upper right of Fig. 10 corresponds to a viscous flux flow regime ($r_d = r_f = \text{const}$), which can only be approached asymptotically.

The resistance of superconductor is determined by the density n of free vortices broken away from pinning centers of Eq. (20). In the special case of exponential cluster area distribution ($g = 0$) the free vortex density is equal to

$$n = \frac{B}{\Phi_0} \exp\left(-C i^{-2/D}\right) \quad (37)$$

The more vortices are free to move, the stronger the induced electric field, and therefore, the higher is the voltage across a sample at the same transport current. If we differentiate the V - I characteristic of Eq. (34) and compare with formula of Eq. (37), we will see that the differential resistance is proportional to the density of free vortices: $r_d = (r_f \Phi_0 / B)n$. Resistance of a superconductor in the resistive state is determined by the motion just

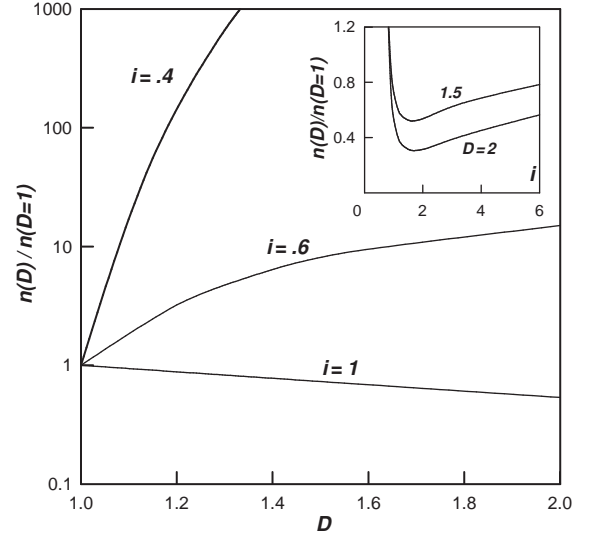


FIG. 11: Dependence of the free vortex density on the fractal dimension of the normal-phase clusters for different values of a transport current. The inset shows the free vortex density versus current for two values of a fractal dimensions.

of these vortices.

Figure 11 demonstrates dependence of the relative density of free vortices $n(D)/n(D = 1)$ (relatively to the value for clusters with Euclidean boundary) on the fractal dimension for different magnitudes of transport currents. The vortices are broken away from pinning centers mostly when $i > 1$, that is to say, above the resistive transition. Here the free vortex density decreases with increasing the fractal dimension. Such a behavior can be explained by the peculiarity of the critical current distribution of Eq. (16). The curve of this distribution broadens out, moving towards greater magnitudes of current as the fractal dimension increases. It means that there are more clusters of high depinning current in superconductor. The smaller part of the vortices is free to move, the smaller the induced electric field. The fact that the fractality of cluster boundary enhances pinning is also demonstrated in Fig. 10, where the resistance decreases with increasing fractal dimension above the resistive transition. The relative change in free vortex density depends on the transport current (see inset in Fig. 11) and, in the limiting case of the most fractal boundary $D = 2$ reaches a minimum for $i = 1.6875$ (this curve should go below others in Fig. 11). That corresponds to the maximum pinning gain and the minimum level of dissipation.

In the range of transport currents below the resistive transition ($i < 1$) the resistance as well as the free vortex density increase for the clusters of greater fractal dimension (see Figs. 10 and 11). Such a behavior is related to the fact that the critical current distribution of Eq. (16) broadens out covering both high and small currents as the fractal dimension increases. For this reason, the breaking of the vortices away under the action of transport

current begins earlier for the clusters of greater fractal dimension. In spite of sharp increase in relative density of free vortices (Fig. 11), the absolute value of vortex density in the range of currents involved is very small (much smaller than above the resistive transition). So the vortex motion does not lead to the destruction of the superconducting state yet, and the resistance remains very low. The low density of vortices at small currents is related to the peculiarity of exponential-hyperbolic distribution of Eq. (16). This function is so “flat” in the vicinity of the coordinate origin that all its derivatives are equal to zero at the point of $i = 0$: $d^k f(0)/di^k = 0$ for any value of k . This mathematical feature has a clear physical meaning: so small a transport current does not significantly affect the trapped magnetic flux because there are scarcely any pinning centers of such small critical currents in the overall statistical distribution, so that nearly all the vortices are still pinned. This interval corresponds to the so-called initial fractal dissipation regime, which was observed in BPSCCO samples with silver inclusions as well as in polycrystalline YBCO and GdBCO samples.¹¹

IX. CONCLUSION

So, in the present work the fractal nature of the normal-phase clusters is revealed, and relation between

the fractal properties of the clusters and dynamics of the trapped magnetic flux is established. The fractal distribution of the critical current is obtained. It is found that the fractality of cluster boundary strengthens the flux pinning and thereby hinders the destruction of superconductivity by the transport current. V - I characteristics of fractal superconducting structures in a resistive state are obtained. It is revealed that the fractality of the boundaries of the normal-phase clusters reduces the electric field arising from magnetic flux motion, and thereby raises the critical current of a superconductor. The fractal properties of the normal-phase clusters significantly affect the resistive transition. This phenomenon is related to the features of the fractal critical current distribution. The resistance characteristics correspond to a mixed state of the vortex glass type. An important result is that the fractality of the normal-phase clusters enhances pinning, thus decreasing the resistance above the resistive transition and increasing the current-carrying capability of a superconductor.

Acknowledgments

This work is supported by the Saint Petersburg Scientific Center of the Russian Academy of Sciences.

-
- * Electronic address: yurk@mail.ioffe.ru, iourk@yandex.ru
- ¹ A. Tonomura, H. Kasai, O. Kamimura, T. Matsuda, K. Harada, Y. Nakayama, J. Shimoyama, K. Kishio, T. Hanaguri, K. Kitazawa, et al., *Nature* **412**, 620 (2001).
 - ² J. Lidmar, D. R. Nelson, and D. A. Gorokhov, *Phys. Rev. B* **64**, 144512 (2001).
 - ³ B. Dam, J. M. Huijbregtse, and J. H. Rector, *Phys. Rev. B* **65**, 064528 (2002).
 - ⁴ T. Higuchi, S. I. Yoo, and M. Murakami, *Phys. Rev. B* **59**, 1514 (1999).
 - ⁵ E. Mezzetti, R. Gerbaldo, G. Ghigo, L. Gozzelino, B. Minetti, C. Camerlingo, A. Monaco, G. Cuttone, and A. Rovelli, *Phys. Rev. B* **60**, 7623 (1999).
 - ⁶ M. R. Beasley, in: *Percolation, Localization and Superconductivity*, ed. by A. M. Goldman and S. A. Wolf, vol. 109 of *NATO ASI Series, Ser. B*, pp. 115-143 (Plenum Press, New York, 1984).
 - ⁷ L. Krusin-Elbaum, G. Blatter, J. R. Thompson, D. K. Petrov, R. Wheeler, J. Ullmann, and C. W. Chu, *Phys. Rev. Lett.* **81**, 3948 (1998).
 - ⁸ Y. I. Kuzmin, *Tech. Phys. Lett.* **26**, 791 (2000).
 - ⁹ C. J. Olson, C. Reichhardt, and F. Nori, *Phys. Rev. Lett.* **80**, 2197 (1998).
 - ¹⁰ R. Surdeanu, R. J. Wijngaarden, B. Dam, J. Rector, R. Griessen, C. Rossel, Z. F. Ren, and J. H. Wang, *Phys. Rev. B* **58**, 12467 (1998).
 - ¹¹ M. Prester, *Phys. Rev. B* **60**, 3100 (1999).
 - ¹² Y. I. Kuzmin, *Phys. Lett. A* **267**, 66 (2000).
 - ¹³ Y. I. Kuzmin, *Phys. Rev. B* **64**, 094519 (2001).
 - ¹⁴ A. E. Pashitski, A. Polyanskii, A. Gurevich, J. A. Parrell, and D. C. Larbalestier, *Physica C* **246**, 133 (1995).
 - ¹⁵ Y. Fukumoto, Q. Li, Y. L. Wang, M. Suenaga, and P. Haldar, *Appl. Phys. Lett.* **66**, 1827 (1995).
 - ¹⁶ M. Suenaga, Y. Fukumoto, P. Haldar, T. R. Thurston, and U. Wildgruber, *Appl. Phys. Lett.* **67**, 3025 (1995).
 - ¹⁷ I. Hlasek, L. Jansak, M. Majoros, J. Kokavec, and F. Chovanec, *IEEE Trans. Magnetics* **32**, 2806 (1996).
 - ¹⁸ A. W. Smith, H. M. Jaeger, T. F. Rosenbaum, W. K. Kwok, and G. W. Crabtree, *Phys. Rev. B* **59**, R11665 (1999).
 - ¹⁹ M. V. Indenbom, M. Konczykowski, C. J. V. D. Beek, and F. Holtzberg, *Physica C* **341-348**, 1251 (2000).
 - ²⁰ G. Blatter, M. V. Feigelman, V. B. Geshkenbein, A. I. Larkin, and V. M. Vinokur, *Rev. Mod. Phys.* **66**, 1125 (1994).
 - ²¹ G. Blatter, V. B. Geshkenbein, and J. A. G. Koopmann, *Phys. Rev. Lett.* **92**, 067009 (2004).
 - ²² K. Yamafuji and T. Kiss, *Physica C* **258**, 197 (1996).
 - ²³ M. Ziese, *Physica C* **269**, 35 (1996).
 - ²⁴ M. Ziese, *Phys. Rev. B* **53**, 12422 (1996).
 - ²⁵ D. J. Scalapino, *Phys. Reports* **250**, 329 (1995).
 - ²⁶ H. R. Kerchner, D. P. Norton, A. Goyal, J. D. Budai, D. K. Christen, D. M. Kroegeer, M. Paranthaman, D. F. Lee, F. A. List, R. Feenstra, et al., *Phys. Rev. B* **60**, 6878 (1999).
 - ²⁷ H. Pastoriza, S. Candia, and G. Nieva, *Phys. Rev. Lett.* **83**, 1026 (1999).
 - ²⁸ H. Kupfer, T. Wolf, A. A. Zhukov, and R. Meier-Hirmer, *Phys. Rev. B* **60**, 7631 (1999).
 - ²⁹ I. Maggio-April, C. Renner, A. Erb, E. Walker, and

- O. Fisher, *Nature* **390**, 487 (1997).
- ³⁰ J. Z. Liu, Y. X. Jia, R. N. Shelton, and M. J. Fluss, *Phys. Rev. Lett.* **66**, 1354 (1991).
- ³¹ M. Oussena, P. A. J. de Groot, S. J. Porter, R. Gagnon, and L. Taillefer, *Phys. Rev. B* **51**, 1389 (1995).
- ³² M. Oussena, P. A. J. de Groot, K. Deligiannis, A. V. Volkobuz, R. Gagnon, and L. Taillefer, *Phys. Rev. Lett.* **76**, 2559 (1996).
- ³³ C. A. Durán, P. L. Gammel, R. Wolfe, V. J. Fratello, D. J. Bishop, J. P. Rice, and D. M. Ginsberg, *Nature (London)* **357**, 474 (1992).
- ³⁴ C. A. Durán, P. L. Gammel, D. J. Bishop, J. P. Rice, and D. M. Ginsberg, *Phys. Rev. Lett.* **74**, 3712 (1995).
- ³⁵ U. Welp, T. Gardiner, D. O. Gunter, B. W. Veal, G. W. Crabtree, V. K. Vlasko-Vlasov, and V. I. Nikitenko, *Phys. Rev. Lett.* **74**, 3713 (1995).
- ³⁶ R. J. Wijngaarden, R. Griessen, J. Fendrich, and W.-K. Kwok, *Phys. Rev. B* **55**, 3268 (1997).
- ³⁷ J. Hanisch, A. Attenberger, B. Holzapfel, and L. Schultz, *Phys. Rev. B* **65**, 052507 (2002).
- ³⁸ A. I. Rykov, S. Tajima, F. V. Kusmartsev, E. M. Forgan, and C. Simon, *Phys. Rev. B* **60**, 7601 (1999).
- ³⁹ T. Schuster, H. Kuhn, M. R. Koblishka, H. Theuss, H. Krommüller, M. Leghissa, M. Kraus, and G. Saemann-Ischenko, *Phys. Rev. B* **47**, 373 (1993).
- ⁴⁰ A. Kilic, K. Kilic, and S. Senoussi, *J. Appl. Phys.* **84**, 3254 (1998).
- ⁴¹ J. E. Sonier, R. F. Kiefl, J. H. Brewer, D. A. Bonn, S. R. Dunsiger, W. N. Hardy, R. Liang, R. I. Miller, D. R. Noakes, and C. E. Stronach, *Phys. Rev. B* **59**, R729 (1999).
- ⁴² F. Spitzer, *Principles of Random Walk* (Princeton, New Jersey, 1964).
- ⁴³ C. W. Gardiner, *Handbook of Stochastic Methods* (Springer-Verlag, Berlin, 1983).
- ⁴⁴ S. N. Dorogovtsev and Y. I. Kuzmin, *Phys. Lett. A* **170**, 245 (1992).
- ⁴⁵ H. Fangohr, S. J. Cox, and P. A. J. de Groot, *Phys. Rev. B* **64**, 064505 (2001).
- ⁴⁶ M. Turchinskaya, D. L. Kaiser, F. W. Gayle, A. J. Shapiro, A. Roytburd, V. Vlasko-Vlasov, A. Polyanskii, and V. Nikitenko, *Physica C* **216**, 205 (1993).
- ⁴⁷ U. Welp, T. Gardiner, D. Gunter, J. Fendrich, G. W. Crabtree, V. K. Vlasko-Vlasov, and V. I. Nikitenko, *Physica C* **235-240**, 241 (1994).
- ⁴⁸ R. P. Feynman and A. R. Hibbs, *Quantum Mechanics and Path Integrals* (McGraw-Hill, New York, 1965).
- ⁴⁹ Y. I. Kuzmin, *Phys. Lett. A* **281**, 39 (2001).
- ⁵⁰ Y. I. Kuzmin, *Phys. Solid State* **43**, 1199 (2001).
- ⁵¹ B. B. Mandelbrot, *Science* **155**, 636 (1967).
- ⁵² B. B. Mandelbrot, *Fractals: Form, Chance, and Dimension* (Freeman, San Francisco, 1977).
- ⁵³ B. B. Mandelbrot, *The Fractal Geometry of Nature* (Freeman, San Francisco, 1982).
- ⁵⁴ B. B. Mandelbrot, in: *Fractals in Physics*, ed. by L. Pietronero and E. Tosatti, pp.3-28 (North-Holland, Amsterdam, 1986).
- ⁵⁵ J. Feder, *Fractals* (Plenum Press, New York, 1988).
- ⁵⁶ A. Sidorenko, C. Surgers, T. Trappmann, and H. von Lohneysen, *Phys. Rev. B* **53**, 11751 (1996).
- ⁵⁷ R. B. Laibowitz, R. F. Voss, and E. I. Alessandrini, in: *Percolation, Localization and Superconductivity*, ed. by A. M. Goldman and S. A. Wolf, vol. 109 of *NATO ASI Series, Ser. B*, pp.145-160 (Plenum Press, New York, 1984).
- ⁵⁸ S. Alexander, *Phys. Rev. B* **27**, 1541 (1983).
- ⁵⁹ D. C. Hong, H. E. Stanley, A. Coniglio, and A. Bunde, *Phys. Rev. B* **33**, 4564 (1986).
- ⁶⁰ R. Pike and H. E. Stanley, *J. Phys. A* **14**, L169 (1981).
- ⁶¹ Y. Gefen, A. Aharony, and S. Alexander, *Phys. Rev. Lett.* **50**, 77 (1983).
- ⁶² S. Havlin and D. Ben-Avraham, *Adv. Phys.* **36**, 695 (1987).
- ⁶³ M. Baziljevich, A. V. Bobyl, H. Bratsberg, R. Deltour, M. E. Gaevski, Y. M. Galperin, V. Gasumyants, T. H. Johansen, I. A. Khrebtov, V. N. Leonov, et al., *J. Phys. (Paris) IV* **6**, 259 (1996).
- ⁶⁴ R. Surdeanu, R. J. Wijngaarden, R. Griessen, C. Rossel, Z. F. Ren, and J. H. Wang, *Physica C* **282-287**, 2219 (1997).
- ⁶⁵ Y. I. Kuzmin, *Tech. Phys. Lett.* **28**, 568 (2002).
- ⁶⁶ Y. I. Kuzmin, *Phys. Lett. A* **300**, 510 (2002).
- ⁶⁷ B. Brown, *Phys. Rev. B* **61**, 3267 (2000).
- ⁶⁸ Y. I. Kuzmin and I. V. Plechakov, *Tech. Phys. Lett.* **25**, 475 (1999).
- ⁶⁹ Y. I. Kuzmin, I. V. Pleshakov, and S. V. Razumov, *Phys. Solid State* **41**, 1594 (1999).
- ⁷⁰ D. Hudson, *Statistics* (CERN, Geneva, 1964).
- ⁷¹ W. H. Warnes and D. C. Larbalestier, *Appl. Phys. Lett.* **48**, 1403 (1986).
- ⁷² R. Wordenweber, *Phys. Rev. B* **46**, 3076 (1992).
- ⁷³ M. P. A. Fisher, *Phys. Rev. Lett.* **62**, 1415 (1989).
- ⁷⁴ D. S. Fisher, M. P. A. Fisher, and D. A. Huse, *Phys. Rev. B* **43**, 130 (1991).